HHS Public Access

Author manuscript

J Am Chem Soc. Author manuscript; available in PMC 2016 September 23.

Published in final edited form as:

J Am Chem Soc. 2015 September 23; 137(37): 12131–12142. doi:10.1021/jacs.5b08027.

Mechanistic Basis for the Bypass of a Bulky DNA Adduct Catalyzed by a Y-Family DNA Polymerase

Rajan Vyas[†,‡], **Georgia Efthimiopoulos**[†,‡], **E. John Tokarsky**[†,§], **Chanchal K. Malik**[‖], **Ashis K. Basu**[‖], and **Zucai Suo**[*,†,§]

[†]Department of Chemistry and Biochemistry, The Ohio State University, Columbus, Ohio, 43210, United States

[§]The Biophysics Ph.D. Program, The Ohio State University, Columbus, Ohio, 43210, United States

[‖]Department of Chemistry, University of Connecticut, Storrs, Connecticut 06269, United States

Abstract

1-Nitropyrene (1-NP), an environmental pollutant, induces DNA damage in vivo and is considered to be carcinogenic. The DNA adducts formed by the 1-NP metabolites stall replicative DNA polymerases but are presumably bypassed by error-prone Y-family DNA polymerases at the expense of replication fidelity and efficiency in vivo. Our running start assays confirmed that a site-specifically placed 8-(deoxyguanosin-N^2-yl)-1-aminopyrene ($dG^{1,8}$), one of the DNA adducts derived from 1-NP, can be bypassed by *Sulfolobus solfataricus* DNA polymerase IV (Dpo4), although this representative Y-family enzyme was paused strongly by the lesion. Pre-steady-state kinetic assays were employed to determine the low nucleotide incorporation fidelity and establish a minimal kinetic mechanism for the $dG^{1,8}$ bypass by Dpo4. To reveal a structural basis for dCTP incorporation opposite $dG^{1,8}$, we solved the crystal structures of the complexes of Dpo4 and DNA containing a templating $dG^{1,8}$ lesion in the absence or presence of dCTP. The Dpo4·DNA-$dG^{1,8}$ binary structure shows that the aminopyrene moiety of the lesion stacks against the primer/template junction pair, while its dG moiety projected into the cleft between the Finger and Little Finger domains of Dpo4. In the Dpo4·DNA-$dG^{1,8}$·dCTP ternary structure, the aminopyrene moiety of the $dG^{1,8}$ lesion, is sandwiched between the nascent and junction base pairs, while its base is present in the major groove. Moreover, dCTP forms a Watson–Crick base pair with dG, two nucleotides upstream from the $dG^{1,8}$ site, creating a complex for "-2" frameshift mutation. Mechanistically, these crystal structures provide additional insight into the aforementioned minimal kinetic mechanism.

[*]**Corresponding Author:**suo.3@osu.edu.

[‡]R.V. and G.E. contributed equally.

ASSOCIATED CONTENT

Supporting Information

The Supporting Information is available free of charge on the ACS Publications website at DOI: 10.1021/jacs.5b08027.

Figures S1-S9 (PDF)

The authors declare no competing financial interest.

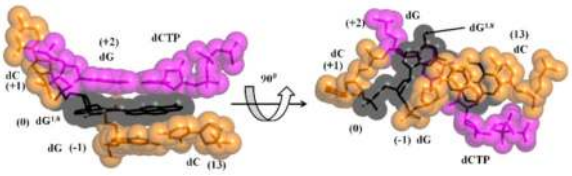

INTRODUCTION

Polycyclic aromatic hydrocarbons (PAHs) are genotoxic environmental contaminants[1] that repetitively damage cellular DNA. 1-Nitropyrene (1-NP), the most abundant nitropolycyclic aromatic compound in the environment,[2–4] is mutagenic[5–7] and carcinogenic.[8,9] It is found in diesel exhaust particulates, coal fly ash, certain grilled foods, as well as emission from wood stoves, fire places, kerosene heaters, and gas burners.[4] Notably, multiple DNA adducts have been reported in rodents treated with 1-NP.[8–11] In humans, 1-NP is mainly metabolized through the nitro reduction pathway (Figure S1). For example, bacteria found in the gastrointestinal tract[12] metabolize 1-NP into DNA-reactive metabolites including *N*-hydroxy-1-aminopyrene (Figure S1).[12,13] Subsequently, *N*-hydroxy-1-aminopyrene is transformed into an electrophilic nitrenium ion which reacts with guanines in DNA to form a major adduct, *N*-(deoxyguanosin-8-yl)-1-aminopyrene (dG^{AP}), and two minor adducts, 8-(deoxyguanosin-N^2-yl)-1-aminopyrene ($dG^{1,8}$) and 6-(deoxyguanosin-N^2-yl)-1-aminopyrene ($dG^{1,6}$) (Figure S1). These DNA adducts are shown to be formed in situ from the reaction of *N*-hydroxy-1-aminopyrene with calf thymus DNA, in vivo by treatment of rat mammary glands with 1-NP, and in vitro by incubating 1-NP with *Salmonella typhimurium* suspension cultures or with rat liver microsomes and cytosols.[14] Moreover, dG^{AP} has been shown to be mutagenic in bacterial and mammalian cells, but the biological effects of the dG-N^2 adducts formed by 1-NP have not been determined.[13,15,16] Since similar dG-N^2 adducts are also formed by several other carcinogenic nitrated PAHs,[17] these dG-N^2 adducts, being representatives of a large group of DNA lesions, are worthy to be further investigated in vitro and in vivo.

In vitro, most DNA adducts are known to stall replicative DNA polymerases because the tight-fitting active sites of these high-fidelity enzymes cannot accommodate DNA lesions, especially those bulky DNA adducts.[18–24] In contrast, the Y-family DNA polymerases, which possess flexible and solvent-accessible active sites, are capable of catalyzing translesion synthesis (TLS) across various DNA lesions and thereby rescuing stalled DNA replication forks in vivo.[25,26] Due to low substrate specificity and lack of a proof-reading exonuclease function, the Y-family DNA polymerases catalyze TLS across most DNA lesions with high error frequency.[26–35] Interestingly, each living organism possesses at least one Y-family DNA polymerase, e.g., there are four in humans (DNA polymerases η, κ, ι, and Rev1), two in *Escherichia coli* (DNA polymerases IV and V), and one in *Sulfolobus solfataricus* (DNA polymerase IV (Dpo4)).[26] Since Dpo4 is in the same subfamily as human DNA polymerase (Pol) κ and *E. coli* Pol IV and shows TLS abilities akin to those of Pol η,[36] it has been intensely studied as a model Y-family enzyme. In vitro, Dpo4 has been shown to bypass numerous bulky DNA adducts including benzo[a]-pyrene diol epoxide (BPDE) on N^2 of deoxyguanosine (dG^{BPDE}) or N^6 of deoxyadenosine (dA^{BPDE}),[37,38] *N*-

(deoxy-guanosin-8-yl)-2-acetylaminofluorene (dG^{AAF}),[39,40] *N*-(deoxy-guanosin-8-yl)-2-aminofluorene (dG^{AF}),[40] and the above-mentioned dG^{AP} adduct.[41] Notably, our recent kinetic and sequencing studies have revealed that Dpo4 and human Y-family enzymes are capable of bypassing a site specifically placed dG^{AP} lesion on a synthetic DNA template in an error-prone manner, although these enzymes are stalled to varying degrees at both the lesion site and a site immediately downstream from the lesion.[41–43] At each of the two pause sites, our kinetic studies also indicate that these polymerases can bind to damaged DNA in either catalytically incompetent ($E{\cdot}DNA_n^D$), nonproductive ($E{\cdot}DNA_n^N$), or productive ($E{\cdot}DNA_n^D$) modes and incorporate dNTP by following a minimal kinetic mechanism in Scheme 1A. Consistently, the crystallographic studies also show different binding conformations of the dG^{AP} lesion within the active site of Dpo4.[44] As a templating nucleotide in the Dpo4·DNA binary complex, dG^{AP} rolls backward and exists in two different extrahelical binding conformations (Figure S2A–B). When the dG^{AP} lesion forms the junction base pair with primer 3′ terminal dC, its aminopyrene ring is also excluded from the DNA helical structure and allows Dpo4, damaged DNA, correct dGTP, and dGMP to form a nonproductive quaternary complex ($E{\cdot}\ DNA_n^N{\cdot}dGTP{\cdot}dGMP$) (Figure S2C).[44] In comparison, a productive ternary conformation ($E{\cdot}DNA_n^P{\cdot}dCTP$) is formed at the active site of human Pol ι with the aminopyrene ring of the templating dG^{AP} lesion expelled out of the DNA double helix[45] (Figure S2D).

Unlike dG^{AP}, the aforementioned 1-NP-derived minor DNA adducts ($dG^{1,6}$ and $dG^{1,8}$) have never been investigated kinetically and structurally. To fill this void, we carried out pre-steady-state kinetic analysis of the bypass of a site-specifically placed $dG^{1,8}$ on a synthetic DNA template by Dpo4. We also crystallized and solved the structures of the binary and ternary complexes of Dpo4 and a DNA substrate containing a $dG^{1,8}$ lesion in the presence or absence of correct dCTP. These comprehensive kinetic and structural studies provide a mechanistic basis for the bypass of $dG^{1,8}$ catalyzed by a model Y-family DNA polymerase.

MATERIALS AND METHODS

Materials

The full-length Dpo4 was expressed in *E. coli* and purified as previously described.[46] Reagents were purchased from the following companies: OptiKinase from USB Corp., [γ-^{32}P]ATP from PerkinElmer, and dNTPs from GE Healthcare.

Synthetic Oligonucleotides

The damaged DNA templates 26-mer-$dG^{1,8}$ and 18-mer-$dG^{1,8}$ (Table 1) were synthesized and purified as previously described.[47] The other DNA oligimers listed in Table 1 were purchased from Integrated DNA Technologies (Coralville, IA) and purified by denaturing polyacrylamide gel electrophoresis (PAGE). The concentration of each purified DNA oligomer was determined through its UV absorbance at 260 nm.

Labeling and Annealing of the DNA Substrates

Each primer was 5′-[^{32}P]-labeled by incubating it with OptiKinase and [γ-^{32}P] ATP for 3 h at 37 °C. The 5′-[^{32}P]-labeled primer was purified and then annealed to an unlabeled

template at a molar ratio of 1.00:1.15. This mixture was first heat denatured at 72 °C for 5 min and then cooled slowly to room temperature over several hours.

Buffers

All pre-steady-state kinetic assays, if not specified, were performed in the optimized reaction buffer R (50 mM HEPES, pH 7.5 at 37 °C, 5 mM $MgCl_2$, 50 mM NaCl, 0.1 mM EDTA, 5 mM DTT, 10% glycerol, and 0.1 mg/mL bovine serum albumin).[46] All electrophoresis mobility shift assays (EMSA) were performed in buffer S (50 mM Tris-Cl, pH 7.5 at 23 °C, 5 mM $MgCl_2$, 50 mM NaCl, 5 mM DTT, 10% glycerol, and 0.1 mg/mL bovine serum albumin). All given concentrations were final after mixing all solutions.

Running Start Assay

The running start assay was performed as previously described.[41] Briefly, a preincubated solution of 5′-[^{32}P]-labeled DNA (100 nM) and Dpo4 (100 nM) in buffer R was rapidly mixed with a solution containing all four dNTPs (200 μM each) at 37 °C via a rapid chemical-quench flow apparatus (KinTek). The reaction was quenched with 0.37 M EDTA after various times, and the reaction products were analyzed by denaturing PAGE (17% polyacrylamide, 8 M urea).

EMSA

Dpo4 (0.5 to 128 nM) was titrated into a solution containing 5'-[^{32}P]-labeled DNA (10 nM) in buffer S at 23 °C. To separate the binary complex from free DNA, native PAGE was conducted at a constant voltage of 70 V for 35 min at 23 °C using running buffer A (50 mM Tris-acetate, pH 7.5 at 23 °C, 0.5 mM EDTA, 5.5 mM $Mg(OAc)_2$). After drying the gel, the bands were quantitated using a Typhoon Trio (GE Healthcare). The dependence of the concentration of the binary complex (Dpo4·DNA) on the total Dpo4 concentration was fit to eq 1 using KaleidaGraph (Synergy Software) to yield $K_{d,\mathrm{DNA}}$, the equilibrium dissociation constant for the binary complex (Dpo4·DNA) at 23 °C.

$$[\mathrm{Dpo4 \cdot DNA}]=0.5(K_{d,\mathrm{DNA}}+E_\mathrm{o}+D_\mathrm{o}) - 0.5$$

$$[(K_{d,\mathrm{DNA}}+E_\mathrm{o}+D_\mathrm{o})^2 - 4E_\mathrm{o}D_\mathrm{o}]^{1/2} \quad (1)$$

In eq 1, E_0 is the total Dpo4 concentration and D_0 the total DNA concentration.

Determination of Nucleotide Incorporation Efficiency

A preincubated solution of Dpo4 (120 nM) and 5′-[^{32}P]-labeled DNA (30 nM) in buffer R was mixed with increasing concentrations of a dNTP. The reactions were terminated after various times using 0.37 M EDTA. Reaction products were analyzed by denaturing PAGE and quantitated with a Typhoon Trio (GE Healthcare). The time course of product formation at each dNTP concentration was fit to a single-exponential equation, eq 2

$$[\mathrm{Product}]=A(1 - \exp(-k_\mathrm{obs}t)) \quad (2)$$

where k_{obs} is the observed reaction rate constant and A is the reaction amplitude. Next, the plot of the k_{obs} versus the dNTP concentration was fit to a hyperbolic equation, eq 3

$$k_{obs}=k_p[dNTP]/\{[dNTP]+K_{d,dNTP}\} \quad (3)$$

where k_p is the maximum dNTP incorporation rate and $K_{d,dNTP}$ is the equilibrium dissociation constant for the ternary complex (Dpo4· DNA·dNTP). Nucleotide incorporation efficiency ($k_p/K_{d,dNTP}$) was then calculated.

Biphasic Kinetic Assay

A preincubated solution of Dpo4 (120 nM) and 5′-[^{32}P]-labeled DNA (30 nM) in buffer R was rapidly mixed with a solution of 5 μM unlabeled DNA trap (Table 1)[46] and 0.2, 0.7, or 1.2 mM correct dNTP in buffer R for various times before being quenched with 0.37 M EDTA. Reaction products were resolved and quantitated as described above. The plot of the product concentration versus reaction time was fit to a double-exponential equation, eq 4

$$[\text{Product}]=E_0A_f[1-\exp(-k_ft)]+E_0A_s[1-\exp(-k_st)] \quad (4)$$

where E_0 is the total Dpo4 concentration, A_f and A_s are the reaction amplitudes of the fast and slow phase, respectively, and k_f and k_s are the rate constants of the fast and slow phases, respectively.

Crystallization and Structure Determination

Purified Dpo4 was concentrated to 20 mg/mL and then mixed with the 13/18-mer (Table 1) at a molar ratio of 1:1.2 in a buffer containing 10 mM HEPES (pH 7.0), 0.5 mM DTT, and 10 mM NaCl to form a binary complex. A preinsertion ternary complex was subsequently formed with the addition of dCTP in the presence of 5 mM $CaCl_2$. Notably, Ca(II), rather than catalytic Mg(II), was used here to trap an incoming dNTP in its preinsertion ternary complex.[48] Crystals were grown using the hanging drop vapor diffusion method with the reservoir solution containing 20 mM Tris-HCl (pH 8.0), 15% PEG3350 (w/v), 60 mM NaCl, 5 mM $CaCl_2$, and 4% glycerol (v/v). Using 25% PEG3350 (w/ v) and 15% ethylene glycol (v/v) in the mother liquor, crystals were flash frozen in liquid nitrogen. X-ray diffraction data was collected using LRL-CAT beamline facilities at Advance Photon Source (APS), Argonne National Laboratory. X-ray diffraction data were processed using HKL-2000.[49] PHASER[50] was used for molecular replacement using PDB 2RDJ devoid of all of the ligand and solvent molecules as the search model. REFMAC5[51] and COOT[52] were used for structural refinement and model building, respectively, which were performed repeatedly for several cycles until there was no further reduction in the R_{work} and R_{free} factors. Quality of the final refined models was assessed using PROCHECK,[53] and figures were created using PYMOL.[54] Atomic coordinates have been deposited in the Protein Data Bank (www.rcsb.org) under an accession code of 4RZR.

RESULTS

Bypass of a Site-Specifically Placed dG[1,8] Lesion Catalyzed by Dpo4 in the Presence of Mg(II)

Running start assays (Materials and Methods) were performed to observe Dpo4-catalyzed DNA polymerization patterns with an undamaged 17/26-mer and a damaged 17/26-mer-dG[1,8] containing a site-specifically placed dG[1,8] lesion in the template (Table 1). Dpo4 copied the undamaged template 26-mer and synthesized the full-length product 26-mer within 180 s (Figure 1A) as reported previously.[41] In contrast, it took 1800 s or a 10-fold longer time for Dpo4 to bypass the dG[1,8] lesion and synthesize the 26-mer (Figure 1B). Notably, the intermediate product 20-mer accumulated with time, indicating that Dpo4 paused and struggled to incorporate a nucleotide opposite the dG[1,8] lesion (Figure 1B). Notably, another intermediate product 25-mer also accumulated to a certain degree with both damaged and undamaged templates (Figure 1). The 25-mer accumulation was likely due to polymerase "slippage" via primer realignment at the dC-rich sequence of the 5′-termini of the damaged and undamaged 26-mer templates (Table 1).[41]

Effect of the dG[1,8] Lesion on DNA Binding to Dpo4 in the Presence of Mg(II)

The 20-mer accumulation in Figure 1B was possibly caused by the weak affinity of 20/26-mer-dG[1,8] to Dpo4. To evaluate this possibility, EMSA (Materials and Methods) was performed to measure the affinities ($1/K_{d,\mathrm{DNA}}$) (Table 2) of several damaged DNA substrates to Dpo4 as previously performed with the undamaged DNA substrates.[41] Figure S3 shows a representative plot for the determination of the $K_{d,\mathrm{DNA}}$ (9.8 ± 0.9 nM) of the binary complex Dpo4·19/26-mer-dG[1,8]. Notably, the data in Table 2 show that Dpo4 bound to various undamaged DNA substrates with comparative affinity (3.1–4.0 nM), whereas the damaged DNA substrates were bound with a broader range of values (9–27 nM). Interestingly, only ~2-fold weaker binding affinity was observed with 20/26-mer-dG[1,8] relative to the undamaged 20/26-mer. Surprisingly, Dpo4 was bound to 21/26-mer-dG[1,8], the DNA substrate at a nonpause site, with ~7-fold weaker affinity than to 21/26-mer. Thus, the binding affinity differences between damaged and undamaged DNA substrates do not correlate well with the polymerase pausing pattern in Figure 1B.

Effect of the dG[1,8] Lesion on Kinetic Parameters of Nucleotide Incorporation in the Presence of Mg(II)

In order to identify a major factor contributing to the polymerase pausing pattern in Figure 1A, we determined the maximum incorporation rate (k_p), the equilibrium dissociation constant ($K_{d,\mathrm{dNTP}}$), and substrate specificity ($k_p/K_{d,\mathrm{dNTP}}$) for nucleotide incorporation opposite each template position under single-turnover conditions (Materials and Methods). For example, a preincubated solution of Dpo4 (120 nM) and 5'-[^{32}P]-labeled 20/26-mer-dG[1,8] (30 nM) was rapidly mixed with dCTP (20–800 μM) and quenched with 0.37 M EDTA at various times. The products were resolved by denaturing PAGE. The product concentration was plotted against reaction time, and the data were fit to eq 2 (Materials and Methods) to determine the observed reaction rate k_{obs} (Figure 2A). The dependence of k_{obs} on dCTP concentration was plotted and fit to eq 3 (Materials and Methods), yielding a k_p of $(1.05 \pm 0.03) \times 10^{-2}$ s^{-1} and a $K_{d,\mathrm{dCTP}}$ of 219 ± 17 μM (Figure 2B). This single-turnover

kinetic assay was repeated for each of the DNA substrates representing the progression of Dpo4 as it approached, encountered, and bypassed the dG[1,8] lesion, and the resulting kinetic data are summarized in Table 3. On the basis of the $k_p/K_{d,\mathrm{dNTP}}$ values, Dpo4 catalyzed dNTP incorporation opposite dG[1,8] with the following efficiency order: dCTP ≫ dTTP > dATP > dGTP. Similarly, correct nucleotides were incorporated more efficiently than any incorrect nucleotides by 2 or 3 orders of magnitude at other template positions (Table 3).

Relative to 20/26-mer, a single dG[1,8] lesion decreased the primer elongation efficiency of 20/26-mer-dG[1,8] by 1188-fold (Table 3), and this decrease was mainly contributed by the 1100-fold k_p drop (Figure S4B). In contrast, the k_p ratios are not large at nonpause sites, while the $K_{d,\mathrm{dNTP}}$ ratios were within 4-fold (Figure S4). The polymerase fidelity, defined as $(k_p/K_{d,\mathrm{dNTP}})_{\mathrm{incorrect}}/[(k_p/K_{d,\mathrm{dNTP}})_{\mathrm{correct}} + (k_p/K_{d,\mathrm{dNTP}})_{\mathrm{incorrect}}]$, at both upstream and downstream positions from the lesion, is in the range from 10^{-3} to 10^{-4} with the exception of dCTP misincorporation (10^{-2} in Table 3) onto 21/26-mer-dG[1,8]. This irregularity was likely caused by dCTP misalignment with the next template nucleotide dGMP (Table 1). Notably, the fidelity is similar to the one (from 10^{-3} to 10^{-4}) determined previously with the corresponding undamaged DNA substrates.[41] However, the dG[1,8] lesion lowered the polymerase fidelity (from 10^{-2} to 10^{-3}, Table 3) by about 10-fold. Consequently, the probability of correct nucleotide incorporation was at or above 98% at the nonpause sites but dropped to 93.4% when Dpo4 bypassed the dG[1,8] lesion. Therefore, the dG[1,8] lesion dramatically altered the kinetics and selectivity of nucleotide incorporation during lesion bypass but had a marginal effect on polymerization at upstream and downstream positions from the lesion.

Biphasic Kinetics of dNTP Incorporation at the Polymerase Pause Site in the Presence of Mg(II)

Previously, a DNA trap assay has been used to demonstrate that dNTP incorporation opposite various lesions follows biphasic kinetics. [41,42,55–57] To obtain more in-depth kinetic information on the effect of dG[1,8] on dNTP incorporation, we used the same DNA trap assay to uncover multiphase kinetics that tend to hide in the above single-turnover dNTP incorporation assay. For this assay, a large molar excess of unlabeled 21/41-mer (D-1, Table 1) was used as the trap to sequester any free Dpo4 that dissociated from a 5′-[^{32}P]-labeled DNA substrate. As expected, the incorporation of dCTP (1.2 mM) opposite dG[1,8] at the polymerase pause site follows biphasic kinetics (Figure 3). The plot of product concentrations versus reaction times was fit to eq 4 (Materials and Methods) to yield the reaction amplitudes of $A_f = 5.4 \pm 0.5$ nM (18%) and $A_s = 18.2 \pm 0.5$ nM (61%) as well as the reaction rate constants of $k_f = 0.043 \pm 0.007$ s^{-1} and $k_s = 0.0019 \pm 0.0001$ s^{-1} for the fast and slow phase, respectively (Table 4). To evaluate if the fast and slow phase kinetic parameters are affected by dCTP concentration, we performed the DNA trap assay with either 0.2 or 0.7 mM dCTP. The plots of the product concentration versus reaction time display similar biphasic kinetic patterns (Figure 3), and the resulting kinetic parameters are listed in Table 4. Notably, both k_f and k_s increased with higher dCTP concentrations, while both A_f and A_s were nearly unchanged.

Similarly, the DNA trap assays were performed with the DNA substrates at nonpause sites (19/26-mer-dG[1,8] and 21/ 26-mer-dG[1,8]) or with the undamaged DNA substrates (19/26-mer, 20/26-mer, and 21/26-mer) in the presence of a correct nucleotide (1.2 mM). The nucleotide incorporation with each of the DNA substrates displayed monophasic kinetics with a reaction amplitude in the range of 76–89% (Table 4). The smaller than 100% reaction amplitude was likely contributed by the dissociation of the Dpo4·DNA complex, incomplete or imperfect annealing of the DNA duplex, the binding of Dpo4 at the blunt end rather than the staggered end of the DNA substrate, or/and experimental errors.[57]

Crystallographic Studies of Dpo4 in Complex with dCTP and DNA Containing a dG[1,8] Lesion in the Presence of Ca(II)

In order to establish a structural basis for polymerase pausing during the dG[1,8] bypass, we cocrystallized Dpo4 in complex with a DNA substrate 13/18-mer-dG[1,8], containing a dG[1,8] lesion as the templating nucleotide (Table 1), dCTP, and Ca(II) (Materials and Methods). After screening multiple crystals, one crystal diffracted X-rays to 2.2 Å resolution (Table 5). This crystal belongs to the trigonal space group ($P3_1$) with two different Dpo4 complex molecules per asymmetric unit. The refined structure shows that one of the molecules is present as a binary complex of Dpo4·13/18-mer-dG[1,8] (Figure 4A), while the other is a ternary complex of Dpo4·13/18-mer-dG[1,8]·dCTP (Figure 5A). Superposition of the two molecules shows small overall structural changes (Figure 6A) with a root-mean-square deviation (RMSD) of 1.72 Å for all protein backbone Cα atoms.

Intriguingly, the Dpo4·13/18-mer-dG[1,8] binary structure (Figure 4) reveals that the bulky dG[1,8] lesion occupied the space for the nascent base pair at the active site and thereby blocked the binding of an incoming nucleotide (Figures 4 and S5). Moreover, the templating dG[1,8] lesion adopted a unique binding conformation with its aminopyrene ring stacking against the primer/template junction pair and the dG moiety positioned away from the nascent base pair and into the cleft between the Finger and Little Finger domains (Figures 4 and 6B). This binding conformation was stabilized by a hydrogen bond (3.0 Å) between the N1 atom of the dG[1,8] lesion and the backbone carbonyl oxygen atom of residue G58 (Figure 4C). Notably, the template 5′-nucleotides upstream from the dG[1,8] lesion were completely disordered and are not modeled in the Dpo4·13/18-mer-dG[1,8] structure.

In the Dpo4·13/18-mer-dG[1,8]·dCTP ternary structure (Figure 5A), dCTP was not covalently attached to the normal primer 13-mer due to the altered active site structure and binding conformations of DNA and the nascent base pair by the presence of both the bulky lesion dG[1,8] (Discussion) and the divalent metal ions Ca(II).[58] Relative to the Dpo4·13/18-mer-dG[1,8] binary structure, the DNA duplex in the Dpo4·13/ 18-mer-dG[1,8]·dCTP ternary structure was translocated by one base pair (Figure 6B), creating enough space for the nascent base pair (Figure 5). Surprisingly, dCTP skipped two template nucleotides and base paired with the upstream nucleotide dG at the +2 position (Table 1) with a distance of 6.3 Å between the α-phosphorus atom of dCTP and the primer 3′-OH (Figure 5). Such a dCTP binding mode will lead to a “-2 frameshift” mutation if the primer and template strands are not realigned during subsequent DNA synthesis. Interestingly, the skipped template nucleotide dC at the +1 position (Table 1) was excluded from the DNA duplex (Figure 5).

This dC exclusion was likely facilitated by the reposition of a structural loop (residues 31–41) in the Finger domain by 2.9–4.4 Å (Figure 6C) from the binary to the ternary structure. Strikingly, the aminopyrene moiety of the dG[1,8] lesion was sandwiched between the nascent base pair and the primer/template junction base pair, while the base of the lesion was present in the major groove (Figure 5B–D). This unusual binding conformation was stabilized by the strong stacking interactions between the aromatic aminopyrene ring of dG[1,8] and the bases of the nascent and junction base pairs. To accommodate this dG[1,8] binding conformation, the primer 3′-terminal nucleotide was tilted and the junction base pair was repositioned by 2.9–7.1 Å from the binary to the ternary structure (Figure 6B). Moreover, the Little Finger domain was rotated by 15.4° after dCTP binding to the Dpo4·13/18-mer-dG[1,8] complex (Figure 6A).

DISCUSSION

Kinetic Basis for the Intermediate Accumulation Pattern Observed with the Bypass of dG[1,8]

The running start assays demonstrate that Dpo4 was able to bypass a site-specifically placed dG[1,8] but took 10-fold longer time to synthesize the full-length product 26-mer with the damaged DNA template than with the undamaged (Figure 1). The slow product formation was due to strong polymerase pausing after the synthesis of 20-mer. The 20-mer accumulation was slightly contributed by the 2-fold weaker DNA binding affinity in the presence of the bulky lesion (Table 2) but predominantly a result of inefficient dCTP incorporation opposite the lesion dG[1,8] on the basis of our pre-steady-state kinetic data in Table 3. The pause pattern can be explained well by the kinetic pattern of series reactions. The nucleotide incorporation efficiency values ($k_p/K_{d,\mathrm{dNTP}}$) in Table 3 illustrate that correct nucleotide incorporation onto 20/26-mer-dG[1,8] ($4.8 \times 10^{-5}\ \mu\mathrm{M}^{-1}\ \mathrm{s}^{-1}$) is approximately 200-fold less efficient than onto 19/ 26-mer-dG[1,8] ($8.0 \times 10^{-3}\ \mu\mathrm{M}^{-1}\ \mathrm{s}^{-1}$). Hence, the formation of the 20-mer from the 19-mer was achieved with 200-fold higher efficiency than the conversion of the 20-mer to the 21-mer, leading to the accumulation of the 20-mer (Figure 1B). In contrast, correct dGTP incorporation onto 21/26-mer-dG[1,8] ($2.8 \times 10^{-4}\ \mu\mathrm{M}^{-1}\ \mathrm{s}^{-1}$) was 6-fold more efficient than correct dCTP incorporation onto 20/26-mer-dG[1,8] (Table 3), resulting in the lack of accumulation of the intermediate product 21-mer (Figure 1B). Similarly, the lack of accumulation of the 22-mer in Figure 1B can be rationalized through 18-fold more efficient conversion of the 22-mer to 23-mer ($5.0 \times 10^{-3}\ \mu\mathrm{M}^{-1}\ \mathrm{s}^{-1}$) than its production from the 21-mer ($2.8 \times 10^{-4}\ \mu\mathrm{M}^{-1}\ s^{-1}$). Thus, the kinetic basis for a polymerase pause site is governed by significantly less efficient elongation of an intermediate than its formation from a one-nucleotide shorter intermediate. The opposite is true for a nonpause site.

Kinetic Mechanism for the bypass of dG[1,8]

The relatively high binding affinity ($K_{d,\mathrm{DNA}}$= 9.8 nM) of 20/26-mer-dG[1,8] to Dpo4 and its only 2-fold lower affinity than undamaged 20/26-mer (Table 2) indicate that the Dpo4·20/26-mer-dG[1,8] complex was stable enough during primer elongation. The DNA trap experiments confirm that the Dpo4·20/26-mer-dG[1,8] complex stayed bound even during the slow reaction phase of dCTP incorporation which displayed biphasic kinetics (Figure 3).

Notably, the total contribution from the fast ($A_f k_f$) and the slow ($A_s k_s$) phases in the presence of 1.2 mM dCTP (Table 4) yields a rate constant of 0.0089 s^{-1} which is equal to the k_{obs} of 0.0089 s^{-1}, estimated using eq 3, 1.2 mM dCTP, and the $K_{d,dCTP}$ and k_p values determined under single-turnover kinetic conditions (Table 4). This suggests that during a single Dpo4·20/26-mer-dG[1,8] binding event, the damaged DNA substrate was converted to 21/26-mer-dG[1,8] at the active site of Dpo4 via either a fast or a slow phase. In contrast, similar DNA trap experiments with the undamaged DNA substrates and the damaged DNA substrates at two nonpause sites only exhibited monophasic kinetics (Table 4). As previously rationalized, DNA trap assay results for the bypass of an abasic site,[55] a cisplatin-d(GpG) adduct,[56] a dG^{AP} lesion,[41] and an *N*-(2′-deoxyguanosin-8-yl)-3-aminobenzanthrone adduct ($dG^{C8\text{-}N\text{-}ABA}$)[57] by Dpo4, the fast phase observed with 20/26-mer-dG[1,8] was due to the formation of a productive complex E·DNA_n^P which was quickly turned over to 21/26-mer-dG[1,8] once dCTP was bound. Notably, with 19-mer, 20-mer, or 21-mer as the primer, the k_f is smaller with the damaged than with the undamaged DNA substrate. This suggests that even in the fast phase, the E·DNA_n^P complex is more productive with the undamaged than with the damaged DNA. In contrast, a nonproductive complex E·DNA_n^N was formed in the slow phase and converted to 21/26-mer-dG[1,8] without dissociation in the presence of dCTP and a large molar excess of unlabeled DNA trap. Furthermore, when dCTP concentration increased from 0.2 to 0.7 and then to 1.2 mM, both the fast and the slow phase rate constants increased while the reaction amplitudes (A_f and A_s) remained constant (Table 4). The latter observation was expected since the dCTP concentration should not affect the binding of DNA and Dpo4. The dependence of the slow and fast rate constants on nucleotide concentration before saturation suggests that both E·DNA_n^N and E·DNA_n^P bound to dNTP to form their ternary complexes (E·DNA_n^N·dNTP, E·DNA_n^P·dNTP) and were then turned over to the product. However, our kinetic data cannot exclude the possibility that E·DNA_n^N was first converted to E·DNA_n^P with a rate constant of k_e before nucleotide binding and incorporation as in Scheme 1A. Since the dCTP concentration variation should not change k_e but did significantly alter k_s (Table 4), this alternative pathway did not play a significant role in the product formation in the slow phase. Notably, the total reaction amplitude with 20/26-mer-dG[1,8] ($A_s + A_f = 79\%$) is smaller than with 20/26-mer (87%) (Table 4). The 8% reaction amplitude difference might be derived from the faster dissociation of 20/26-mer-dG[1,8] from Dpo4 than 20/26-mer or the formation of a small percentage of a catalytically incompetent complex (E·DNA_n^D) between 20/26-mer-dG[1,8] and Dpo4. Taken together, the above analysis allows us to modify the minimal kinetic mechanism in Scheme 1A and propose a new one in Scheme 1B for the bypass of dG[1,8] catalyzed by Dpo4. This new mechanism is likely more accurate than the one in Scheme 1A to explain the bypass of an abasic site,[55] a cisplatin-d(GpG) adduct,[56] a dG^{AP} lesion,[41] and a $dG^{C8\text{-}N\text{--}ABA}$ lesion[57] by Dpo4 and the bypass of a dG^{AP} lesion by human Y-family DNA polymerases.[42]

Effect of a dG[1,8] Lesion on the Binary Structure of Dpo4 and DNA

Superimposing the binary structures of Dpo4 and undamaged DNA (Dpo4·DNA) (PDB code 2RDJ)[59] and Dpo4·13/18-mer-dG[1,8] (Figure 4A) reveals that the dG[1,8] lesion did not significantly alter the overall protein structure, although there were small domain movements with an RMSD of 1.31 Å for the aligned protein backbone Cα atoms (Figure 7A). In contrast, the DNA substrate shows different binding conformations in the two binary

structures (Figure 7B). Specifically, the base positions of the template and primer strands in the structure of Dpo4·13/18-mer-dG[1,8] are shifted by 2.6–4.1 Å with respect to the corresponding base positions in the structure of Dpo4·DNA, while the phosphate backbone positions are altered by 1.6–6.4 Å. As a result, the primer 3′-OH moves its position by 4.9 Å (Figure 7C). In addition, the undamaged templating nucleotide dT in the Dpo4·DNA structure is extrahelical, while the damaged templating dG[1,8] is placed within the DNA double helix with its aminopyrene moiety stacked with the primer/template junction base pair and its dG moiety sitting at the major groove (Figure 7C). Similar stacking interactions have been observed in one of the binding conformations of the dG[AAF] lesion at the active site of *S. cerevisiae* Pol η (Figure S6B).[60] Together, the differences between the binary structures of Dpo4·13/18-mer-dG[1,8] and Dpo4·DNA likely contribute to the 2-fold binding affinity difference of damaged 20/26-mer-dG[1,8] and undamaged 20/26-mer to Dpo4 (Table 2). Furthermore, although it is likely that the binary structure Dpo4·DNA represents E·DNA$_n^P$ in Scheme 1, it is unclear if the Dpo4·13/18-mer-dG[1,8] structure reflects the binding conformation of either E·DNA$_n^N$ or E· DNA$_n^D$ in the minimal kinetic mechanisms. This uncertainty warrants further studies.

Significant Impact of dG[1,8] on the Ternary Structure of Dpo4, DNA, and dNTP

Overlaying the ternary structure of Dpo4·13/18-mer-dG[1,8]·dCTP (Figure 5A) with our previously published ternary structure of Dpo4, undamaged DNA, and dCTP in the presence of Ca(II) (Dpo4·DNA· dCTP)[48] reveals that the Little Finger domain is rotated by 25.3° from the undamaged to damaged DNA ternary structure, although the other three domains do not significantly alter their positions (Figure 8A). When zoomed into the active site, these structures display both similarities and differences (Figure 8B and 8C). For instance, the nascent base pair in both ternary structures forms Watson–Crick hydrogen bonds, and the triphosphate moiety of dCTP is in a chairlike conformation.[48,61] However, the presence of the dG[1,8] lesion significantly alters the positions of the DNA substrate including the junction base pair, the nascent base pair, two divalent metal ions, and several active site residues. The strong stacking interactions in the sandwich formed from the aminopyrene moiety of the lesion, the nascent base pair, and the primer/template junction base pair shorten the separation of the nascent (2.2–2.5 Å) and junction (3.9–4.1 Å) base pairs by ~6.4 Å. The distance between the α-phosphorus atom and the primer 3′-OH group is 6.3 and 5.0 Å in the damaged and undamaged DNA ternary structures, respectively. The metal ions at sites A and B are respectively shifted by 2.2 and 1.0 Å by the presence of the dG[1,8] lesion. Furthermore, the stacking of the dG[1,8] lesion with the nascent and junction base pairs displaces its guanine base into the major groove, forces a template nucleotide dC at +1 position excluded from the DNA double helix, and alters the position of the structural loop (residues 31–41) of the Finger domain by 3.3–4.8 Å. In conclusion, the presence of the bulky dG[1,8] lesion significantly alters the geometry of the active site and surely affects the catalytic competency of the ternary complex. This conclusion is supported by the significantly lower rate and efficiency of dCTP incorporation opposite dG[1,8] than opposite undamaged dG (Table 3). Thus, it is likely that the Dpo4·13/18-mer-dG[1,8]·dCTP structure represents the binding conformation of E·DNA$_n^N$·dNTP in Scheme 1B.

Different Binding Conformations of Bulky dG Lesions within Polymerase Active Sites

Both binary and ternary structures (Figures 4 and 5) show that the aminopyrene ring of the $dG^{1,8}$ lesion stacks on the primer/template junction base pair. Such a binding mode does not apply to the aminopyrene ring of the dG^{AP} lesion, which is looped out of the DNA double helix within the active site of Dpo4 in the presence or absence of dNTP (Figure S2A–C).[44] Although the aminopyrene ring of the dG^{AP} lesion is also excluded from the DNA helical structure, the guanine base of the templating lesion forms a Watson-Crick base pair with incoming dCTP at the active site of human Pol ι (Figure S2D).[45] An embedded dG^{BPDE} lesion can be either intercalated or flipped out of the DNA double helix at the active site of Dpo4, allowing an incoming dNTP to base pair with the 5′-nucleotide from the adduct (Figure S7).[37] Similar binding conformations have also been observed with an embedded dA^{BPDE} adduct (Figure S8)[38] and dG^{AF} adduct (Figure S9)[40] at the active site of Dpo4. Notably, none of the above-mentioned bulky lesions induce the exclusion of the undamaged template nucleotide at the +1 position as we observed with $dG^{1,8}$ in Figure 5. Nevertheless, it is clear that a Y-family DNA polymerase will manage to use its flexible and solvent-accessible active site to accommodate and bypass bulky DNA lesions. Exclusion of one or more unpaired template nucleotides from the DNA double-helix during the lesion bypass and/or extension steps will result in frameshift mutations.[40] The binding conformation of an excluded bulky adduct can sometimes be stabilized by its interactions with active site residues but will hinder DNA translocation during DNA polymerization.[45] Relative to the ternary structures with undamaged DNA, the aforementioned bulky lesions more or less affect the geometry of the polymerase active site and thereby decrease nucleotide incorporation efficiency (Table 3).

Biological Implication of Our Studies

1-NP, known to cause tumor formation in animal models,[9,62] preferentially reacts with guanines in DNA to form different bulky DNA adducts (Figure S1). These bulky adducts are likely repaired by nucleotide excision repair (NER) in mammalian cells.[63–65] If not repaired, these bulky dG adducts will stall a high-fidelity replicative DNA polymerase, which has a tight and an inflexible active site, in cellular replication machinery. The stalled replicative polymerase then dissociates from DNA, allowing a translesion polymerase to bind and bypass the lesion.[66] Soon after bypassing the lesion, the processive replicative polymerase returns to continue DNA replication. In all living organisms, the translesion synthesis is catalyzed mostly by the Y-family polymerases due to their flexible and spacious active sites.[25,26] Consistently, Dpo4, a model and lone Y-family DNA polymerase in *S. solfataricus*, indeed bypassed the bulky $dG^{1,8}$ (Figure 1B), but its fidelity at the lesion site is 10-fold lower than at undamaged sites (Table 3). Interestingly, the dATP:$dG^{1,8}$ misincorporation by Dpo4 occurred with a high probability (1.9%, Table 3). If a mammalian Y-family polymerase bypasses $dG^{1,8}$ similarly as Dpo4, it will cause G-to-T transversions in vivo as observed with dG^{AP}.[67] Further research is warranted to investigate this possibility and the mutagenic profile of $dG^{1,8}$ in mammalian cells. It is also worth noting that Pol κ has been found to be involved in the postincision steps of NER of bulky lesions in mouse and human cells.[68,69] Thus, a lesion bypass Y-family polymerase in mammalian cells may participate in multiple pathways to handle a bulky DNA lesion like $dG^{1,8}$.

SUMMARY

The running start assays demonstrate that Dpo4 is able to bypass a site-specifically placed $dG^{1,8}$ lesion, although it paused strongly. We employed the pre-steady-state kinetic assays to establish a kinetic basis for the observed intermediate product accumulation pattern and polymerase pausing. Our crystallographic studies revealed unusual binding conformations of a damaged DNA substrate, especially the templating $dG^{1,8}$ lesion, at the active site of Dpo4 during the lesion bypass stage. They also provided important structural insight for the proposed complexes in our minimal kinetic mechanism for the $dG^{1,8}$ bypass. However, more structural studies are required to establish a structural basis for efficient extension steps of the lesion bypass product.

Supplementary Material

Refer to Web version on PubMed Central for supplementary material.

ACKNOWLEDGMENTS

This work was supported by a National Institutes of Health grant (ES009127) to Z.S. and A.K.B. and National Science Foundation grant (MCB-0960961) to Z.S. The authors are grateful for the usage of the Advanced Photon Source, an Office of Science User Facility operated for the U.S. Department of Energy (DOE) Office of Science by Argonne National Laboratory, which was supported by the U.S. DOE under Contract No. DE-AC02-06CH11357. The authors are also grateful for the usage of the Lilly Research Laboratories Collaborative Access Team (LRL-CAT) beamline at Sector 31 of the Advanced Photon Source provided by Eli Lilly Company, which operates the facility.

REFERENCES

1. Rosenkranz HS, Mermelstein R. Mutat. Res., Rev. Genet. Toxicol. 1983; 114:217.
2. Pitts JN Jr, Van Cauwenberghe KA, Grosjean D, Schmid JP, Fitz DR, Belser WL, Knudson GP, Hynds PM. Science. 1978; 202:515. [PubMed: 705341]
3. Rosenkranz HS, McCoy EC, Sanders DR, Butler M, Kiriazides DK, Mermelstein R. Science. 1980; 209:1039. [PubMed: 6996095]
4. Tokiwa H, Kitamori S, Takahashi K, Ohnishi Y. Mutat. Res., Genet. Toxicol. Test. 1980; 77:99.
5. Li AP, Dutcher JS. Mutat. Res. Lett. 1983; 119:387.
6. Mermelstein R, Kiriazides DK, Butler M, McCoy EC, Rosenkranz HS. Mutat. Res., Genet. Toxicol. Test. 1981; 89:187.
7. Purohit V, Basu AK. Chem. Res. Toxicol. 2000; 13:673. [PubMed: 10956054]
8. Hirose M, Lee MS, Wang CY, King CM. Cancer Res. 1984; 44:1158. [PubMed: 6692400]
9. El-Bayoumy K, Hecht SS, Sackl T, Stoner GD. Carcinogenesis. 1984; 5:1449. [PubMed: 6488469]
10. Smith BA, Korfmacher WA, Beland FA. Carcinogenesis. 1990; 11:1705. [PubMed: 2208586]
11. Mitchell CE. Carcinogenesis. 1988; 9:857. [PubMed: 3365847]
12. Rafil F, Franklin W, Heflich RH, Cerniglia CE. Appl. Environ. Microbiol. 1991; 57:962. [PubMed: 2059053]
13. Sabbioni G, Jones CR. Biomarkers. 2002; 7:347. [PubMed: 12437855]
14. Herreno-Saenz D, Evans FE, Beland FA, Fu PP. Chem. Res. Toxicol. 1995; 8:269. [PubMed: 7766811]
15. Mitchelmore CL, Livingstone DR, Chipman JK. Biomarkers. 1998; 3:21. [PubMed: 23899254]
16. Malia SA, Vyas RR, Basu AK. Biochemistry. 1996; 35:4568. [PubMed: 8605207]
17. Fu PP, Herreno-Saenz DJ. Environ. Sci. Health C Environ. Carcinog. Ecotoxicol. Rev. 1999; 17:1.

18. Liu Y, Yang Z, Utzat CD, Liu Y, Geacintov NE, Basu AK, Zou Y. Biochem. J. 2005; 385:519. [PubMed: 15362978]
19. Zou Y, Shell SM, Utzat CD, Luo C, Yang Z, Geacintov NE, Basu AK. Biochemistry. 2003; 42:12654. [PubMed: 14580212]
20. Duvauchelle JB, Blanco L, Fuchs RP, Cordonnier AM. Nucleic Acids Res. 2002; 30:2061. [PubMed: 11972346]
21. Wang L, Broyde S. Nucleic Acids Res. 2006; 34:785. [PubMed: 16452300]
22. Kunkel TA. J. Biol. Chem. 2004; 279:16895. [PubMed: 14988392]
23. Freisinger E, Grollman AP, Miller H, Kisker C. EMBO J. 2004; 23:1494. [PubMed: 15057282]
24. Hogg M, Wallace SS, Doublie S. EMBO J. 2004; 23:1483. [PubMed: 15057283]
25. Mizukami S, Kim TW, Helquist SA, Kool ET. Biochemistry. 2006; 45:2772. [PubMed: 16503632]
26. Maxwell BA, Suo Z. Biochemistry. 2014; 53:2804. [PubMed: 24716482]
27. Masutani C, Kusumoto R, Yamada A, Dohmae N, Yokoi M, Yuasa M, Araki M, Iwai S, Takio K, Hanaoka F. Nature. 1999; 399:700. [PubMed: 10385124]
28. Matsuda T, Bebenek K, Masutani C, Hanaoka F, Kunkel TA. Nature. 2000; 404:1011. [PubMed: 10801132]
29. Levine RL, Miller H, Grollman A, Ohashi E, Ohmori H, Masutani C, Hanaoka F, Moriya M. J. Biol. Chem. 2001; 276:18717. [PubMed: 11376002]
30. Bebenek K, Tissier A, Frank EG, McDonald JP, Prasad R, Wilson SH, Woodgate R, Kunkel TA. Science. 2001; 291:2156. [PubMed: 11251121]
31. Johnson RE, Washington MT, Haracska L, Prakash S, Prakash L. Nature. 2000; 406:1015. [PubMed: 10984059]
32. Zhang Y, Yuan F, Xin H, Wu X, Rajpal DK, Yang D, Wang Z. Nucleic Acids Res. 2000; 28:4147. [PubMed: 11058111]
33. Wang Z. Mutat. Res., DNA Repair. 2001; 486:59. [PubMed: 11425512]
34. Fiala KA, Abdel-Gawad W, Suo Z. Biochemistry. 2004; 43:6751. [PubMed: 15157109]
35. Fiala KA, Suo Z. Biochemistry. 2004; 43:2116. [PubMed: 14967051]
36. Zhang Y, Wu X, Guo D, Rechkoblit O, Geacintov NE, Wang Z. Mutat. Res., Fundam. Mol. Mech. Mutagen. 2002; 510:23.
37. Bauer J, Xing G, Yagi H, Sayer JM, Jerina DM, Ling H. Proc. Natl. Acad. Sci. U. S. A. 2007; 104:14905. [PubMed: 17848527]
38. Ling H, Sayer JM, Plosky BS, Yagi H, Boudsocq F, Woodgate R, Jerina DM, Yang W. Proc. Natl. Acad. Sci. U. S. A. 2004; 101:2265. [PubMed: 14982998]
39. Boudsocq F, Iwai S, Hanaoka F, Woodgate R. Nucleic Acids Res. 2001; 29:4607. [PubMed: 11713310]
40. Rechkoblit O, Kolbanovskiy A, Malinina L, Geacintov NE, Broyde S, Patel DJ. Nat. Struct. Mol. Biol. 2010; 17:379. [PubMed: 20154704]
41. Sherrer SM, Brown JA, Pack LR, Jasti VP, Fowler JD, Basu AK, Suo Z. J. Biol. Chem. 2009; 284:6379. [PubMed: 19124465]
42. Sherrer SM, Sanman LE, Xia CX, Bolin ER, Malik CK, Efthimiopoulos G, Basu AK, Suo Z. Chem. Res. Toxicol. 2012; 25:730. [PubMed: 22324639]
43. Sherrer SM, Taggart DJ, Pack LR, Malik CK, Basu AK, Suo Z. Mutat. Res., Fundam. Mol. Mech. Mutagen. 2012; 737:25.
44. Kirouac KN, Basu AK, Ling H. J. Mol. Biol. 2013; 425:4167. [PubMed: 23876706]
45. Kirouac KN, Basu AK, Ling H. Nucleic Acids Res. 2013; 41:2060. [PubMed: 23268450]
46. Fiala KA, Suo Z. Biochemistry. 2004; 43:2106. [PubMed: 14967050]
47. Chakraborti D, Colis L, Schneider R, Basu AK. Org. Lett. 2003; 5:2861. [PubMed: 12889893]
48. Gaur V, Vyas R, Fowler JD, Efthimiopoulos G, Feng JY, Suo Z. Nucleic Acids Res. 2014; 42:9984. [PubMed: 25104018]
49. Otwinowski Z, Minor W. Methods Enzymol. 1997; 276:307.
50. McCoy AJ, Grosse-Kunstleve RW, Adams PD, Winn MD, Storoni LC, Read RJ. J. Appl. Crystallogr. 2007; 40:658. [PubMed: 19461840]

51. Murshudov GN, Skubak P, Lebedev AA, Pannu NS, Steiner RA, Nicholls RA, Winn MD, Long F, Vagin AA. Acta Crystallogr., Sect. D: Biol. Crystallogr. 2011; 67:355. [PubMed: 21460454]
52. Emsley P, Cowtan K. Acta Crystallogr., Sect. D: Biol. Crystallogr. 2004; 60:2126. [PubMed: 15572765]
53. Laskowski RA, Rullmannn JA, MacArthur MW, Kaptein R, Thornton JM. J. Biomol. NMR. 1996; 8:477. [PubMed: 9008363]
54. DeLano, WL. PYMOL. San Carlos, CA: DeLano Scientific; 2002.
55. Fiala KA, Hypes CD, Suo Z. J. Biol. Chem. 2007; 282:8188. [PubMed: 17210571]
56. Brown JA, Newmister SA, Fiala KA, Suo Z. Nucleic Acids Res. 2008; 36:3867. [PubMed: 18499711]
57. Gadkari VV, Tokarsky EJ, Malik CK, Basu AK, Suo Z. DNA Repair. 2014; 21:65. [PubMed: 25048879]
58. Irimia A, Zang H, Loukachevitch LV, Eoff RL, Guengerich FP, Egli M. Biochemistry. 2006; 45:5949. [PubMed: 16681366]
59. Wong JH, Fiala KA, Suo Z, Ling H. J. Mol. Biol. 2008; 379:317. [PubMed: 18448122]
60. Schorr S, Schneider S, Lammens K, Hopfner KP, Carell T. Proc. Natl. Acad. Sci. U. S. A. 2010; 107:20720. [PubMed: 21076032]
61. Vaisman A, Ling H, Woodgate R, Yang W. EMBO J. 2005; 24:2957. [PubMed: 16107880]
62. Hirose M, Lee MS, Wang CY, King CM. Cancer Res. 1984; 44:1158. [PubMed: 6692400]
63. Wood RD. Annu. Rev. Biochem. 1996; 65:135. [PubMed: 8811177]
64. Sancar A. Annu. Rev. Biochem. 1996; 65:43. [PubMed: 8811174]
65. Lindahl T, Wood RD. Science. 1999; 286:1897. [PubMed: 10583946]
66. Maxwell BA, Suo Z. Biochemistry. 2012; 51:3485. [PubMed: 22471521]
67. Watt DL, Utzat CD, Hilario P, Basu AK. Chem. Res. Toxicol. 2007; 20:1658. [PubMed: 17907783]
68. Ogi T, Lehmann AR. Nat. Cell Biol. 2006; 8:640. [PubMed: 16738703]
69. Ogi T, Limsirichaikul S, Overmeer RM, Volker M, Takenaka K, Cloney R, Nakazawa Y, Niimi A, Miki Y, Jaspers NG, Mullenders LH, Yamashita S, Fousteri MI, Lehmann AR. Mol. Cell. 2010; 37:714. [PubMed: 20227374]

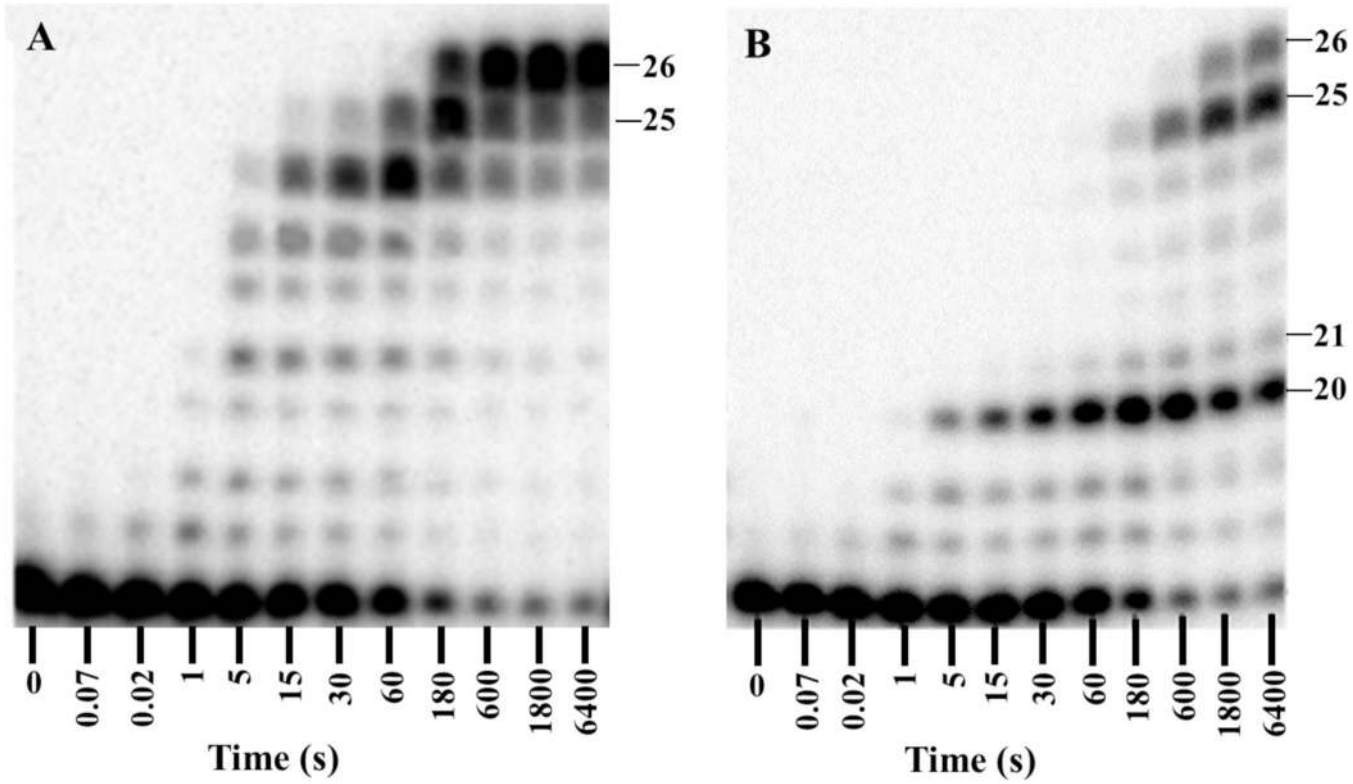

Figure 1.

Running start assays at 37 °C. A preincubated solution of Dpo4 (100 nM) and 5′-^{32}P-labeled DNA substrate (100 nM) was rapidly mixed with a solution containing all four dNTPs (200 μM each), and the reaction was quenched at various times with 0.37 M EDTA. (A) 17/26-mer; (B) 17/26-mer-dG^{1,8}. Size of the important intermediate products are indicated.

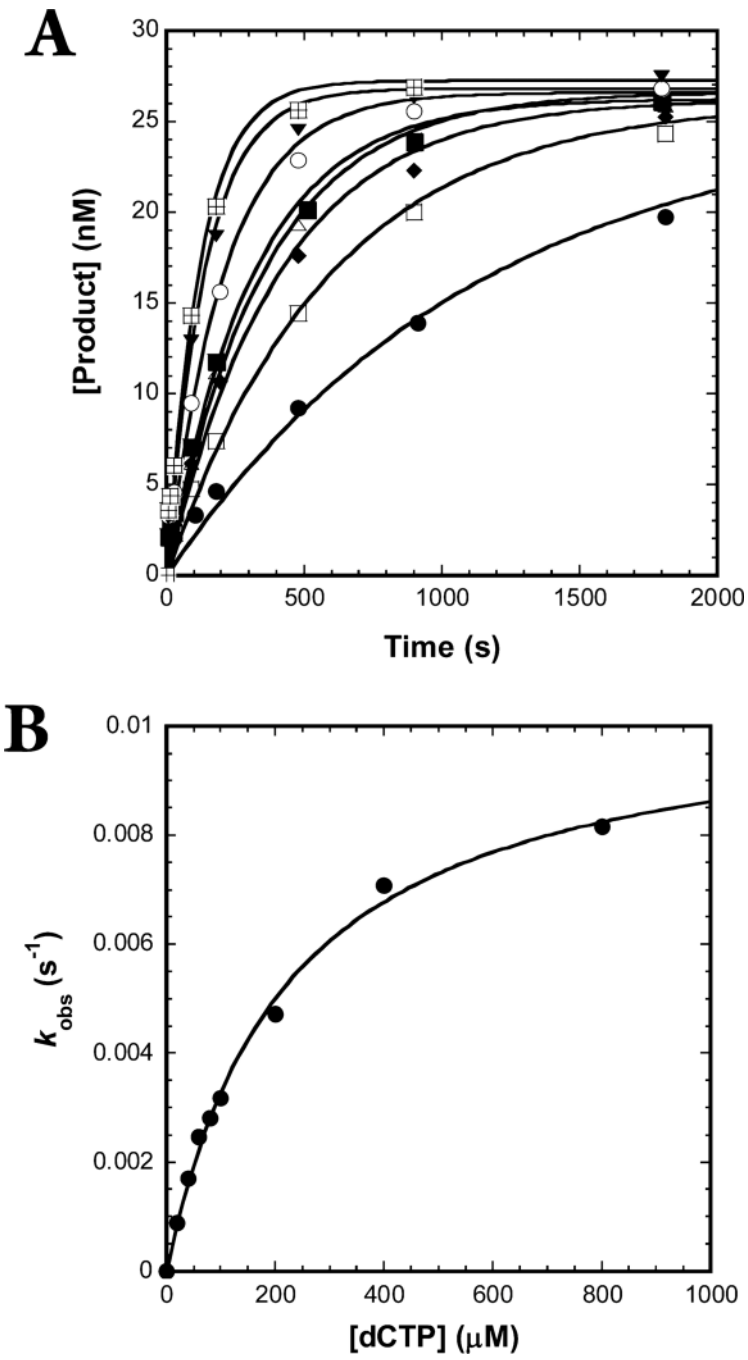

Figure 2.

Pre-steady-state kinetics of dCTP incorporation onto 20/26-mer-dG[1,8]. A preincubated solution of Dpo4 (120 nM) and 5'-[^{32}P]-labeled 20/26-mer-dG [1,8] (30 nM) was rapidly mixed with dCTP (20–800 μM) for various times before being quenched with 0.37 M EDTA. (A) Product concentration was plotted against time, and data were fit to eq 2 (Materials and Methods) to determine k_{obs}. dCTP concentrations are denoted as (●) 20, (D) 40, (♦) 60, (Δ) 80, (■) 100, (○) 200, (▼) 400, and (⊞) 800 μM. (B) Dependence of k_{obs} on

dCTP concentration was plotted and fit to eq 3 (Materials and Methods), which yielded a k_p of $(1.05 \pm 0.03) \times 10^{-2}$ s^{-1} and a $K_{d,dCTP}$ of 219 ± 17 μM.

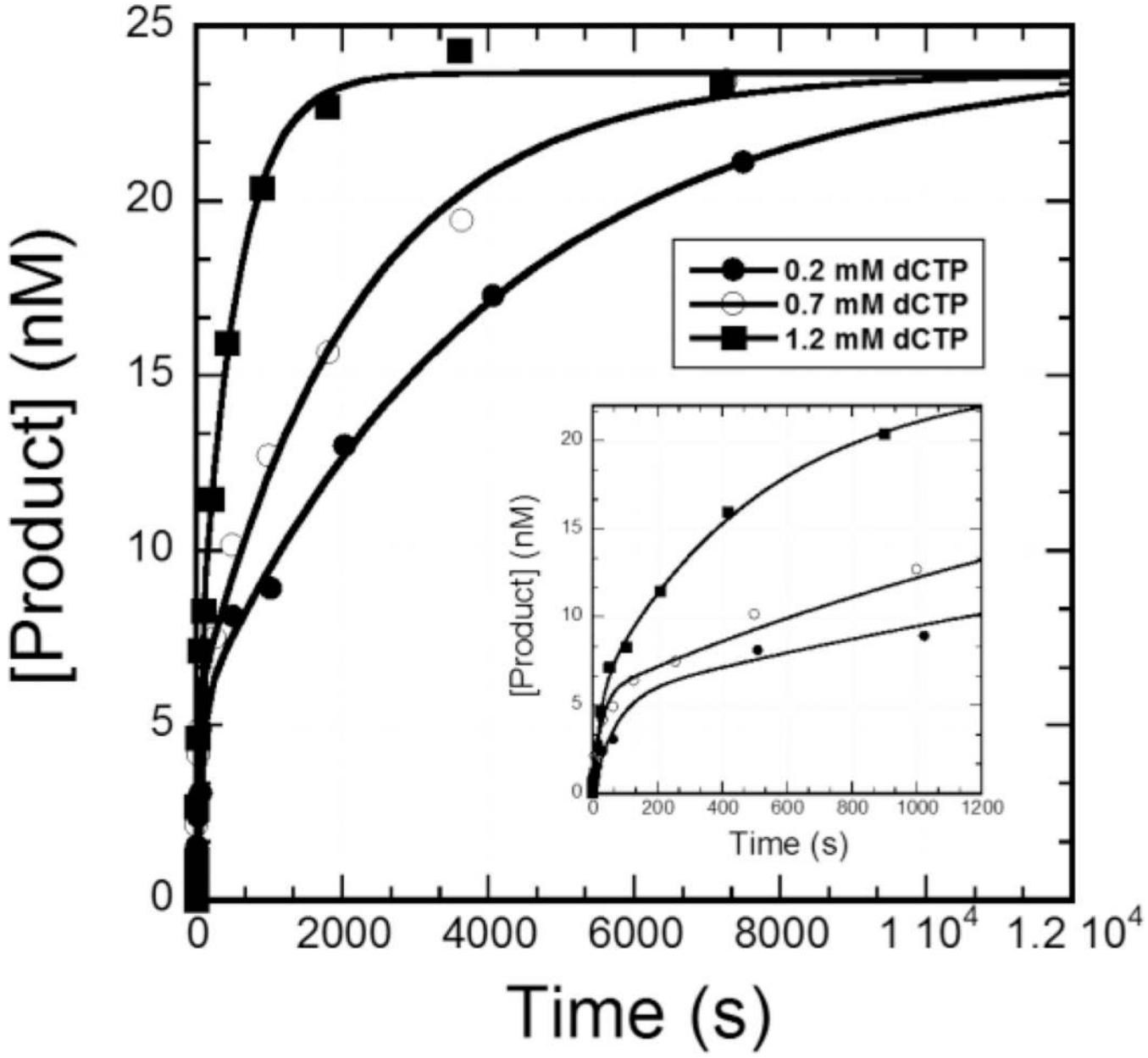

Figure 3.

Biphasic kinetics of dCTP incorporation opposite $dG^{1,8}$ in the presence of a DNA trap. A preincubated solution of Dpo4 (120 nM) and 5'-[^{32}P]-labeled 20/26-mer-$dG^{1,8}$ was mixed rapidly with an unlabeled DNA trap D-1 (5 μM, Table 1) and dCTP (●) 0.2, (○) 0.7, or (■) 1.2 mM). The reaction was quenched with 0.37 M EDTA after various times. Product concentration at each dCTP concentration was first plotted as a function of reaction time, and the plot was then fit to eq 4 (Materials and Methods) to yield kinetic parameters for both the fast and the slow phases (Table 4). (Inset) Magnification of the plots within 1200 s.

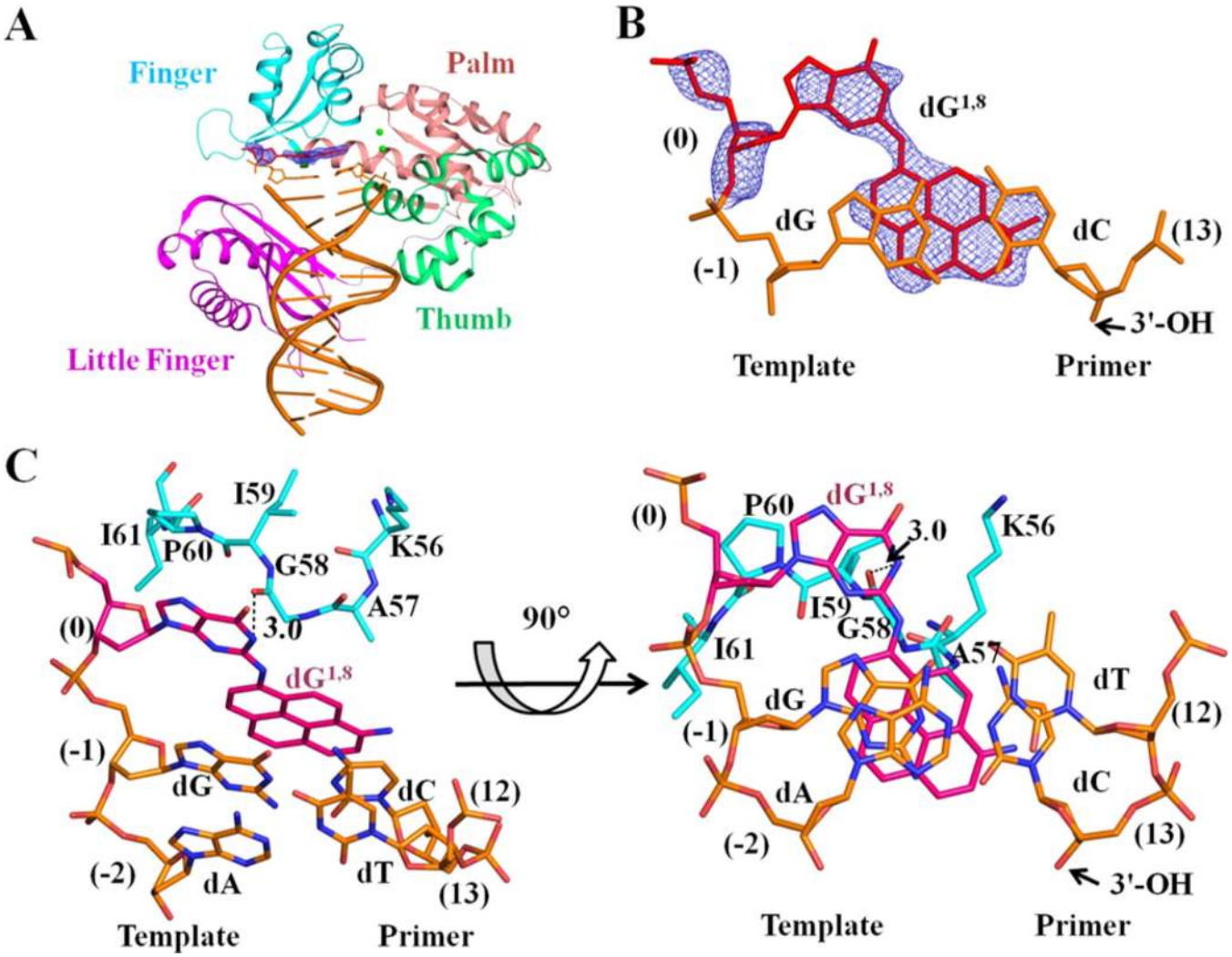

Figure 4.

Binding conformation of the $dG^{1,8}$ lesion in the binary crystal structure of Dpo4·13/18-mer-$dG^{1,8}$. (A) Overall structure with denoted domain names of Dpo4. The $F_o - F_c$ omit map (blue mesh), contoured at the 3σ level, is for the templating $dG^{1,8}$ lesion. (B) Zoomed view of both the electron density map for the $dG^{1,8}$ lesion and the primer/template junction base pair. The aminopyrene ring of the lesion is stacked with the junction base pair. (C) Base N_1 atom of the $dG^{1,8}$ lesion interacts with the carbonyl oxygen atom of the G58 residue of Dpo4. Two different views of the zoomed structure are to show the unusual conformation of the $dG^{1,8}$ lesion.

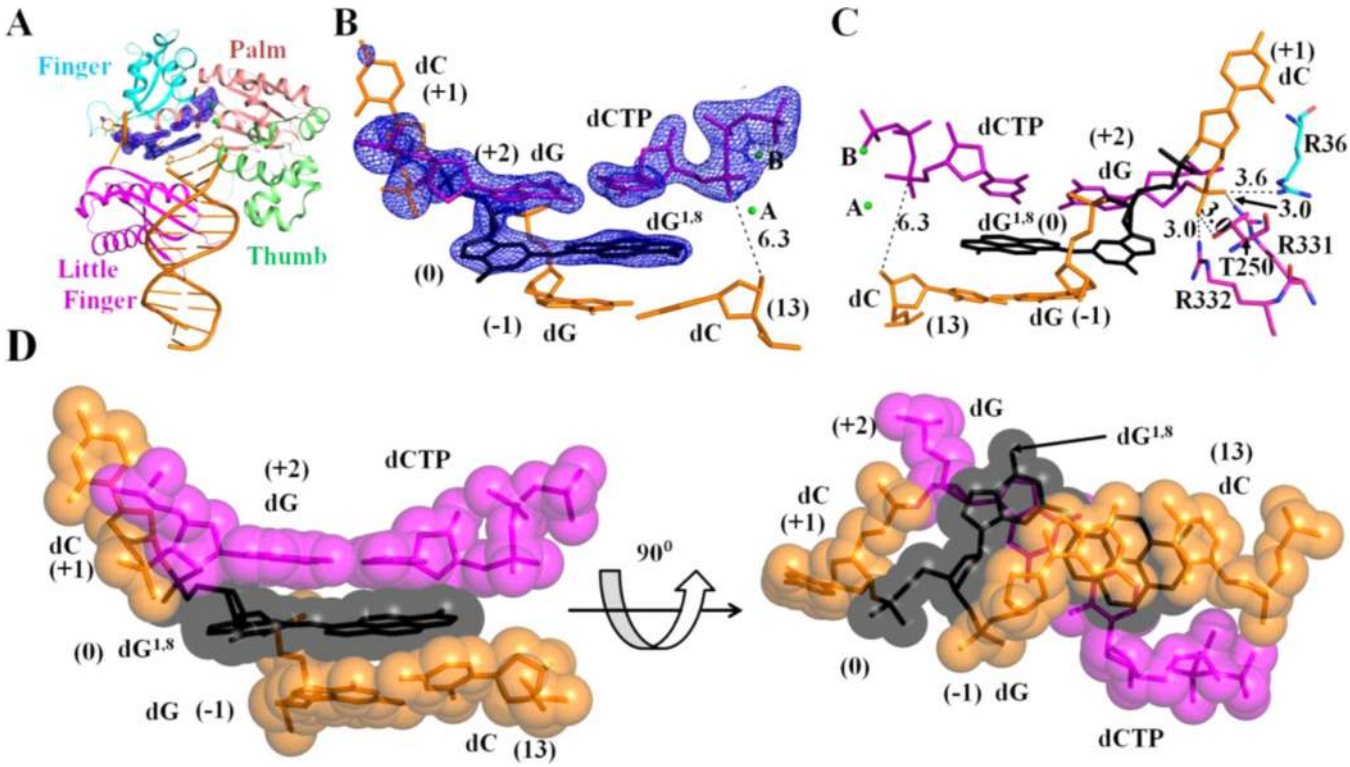

Figure 5.

Binding conformation of $dG^{1,8}$ in the ternary crystal structure of Dpo4·13/18-mer-$dG^{1,8}$·dCTP. (A) Overall crystal structure with the denoted domain names. The $F_o - F_c$ omit map (blue mesh), contoured at the 3σ level, is shown for the nascent base pair at template position +2, the looped-out dC at template position +1, and the $dG^{1,8}$ lesion at template position 0. (B) Zoomed view of the nascent and primer/template junction base pairs. The aminopyrene moiety of the $dG^{1,8}$ lesion stacks between the nascent and the junction base pairs. (C) Zoomed view of the active site to clearly show the looped-out template nucleotide at template position +1 and its interactions with the residues of Dpo4. (D) Zoomed view to show the Watson–Crick base pairing between dCTP and dG at template position +2 (magenta). Nascent base pair formation is facilitated by looping out dC at template position +1 (orange). $dG^{1,8}$ lesion at template position 0 (black) and junction base pair at template position −1 (orange) are also shown. In A-C, the two Ca^{2+} ions at sites A and B are presented as green spheres, and all dashed lines indicate the distances in Angstroms.

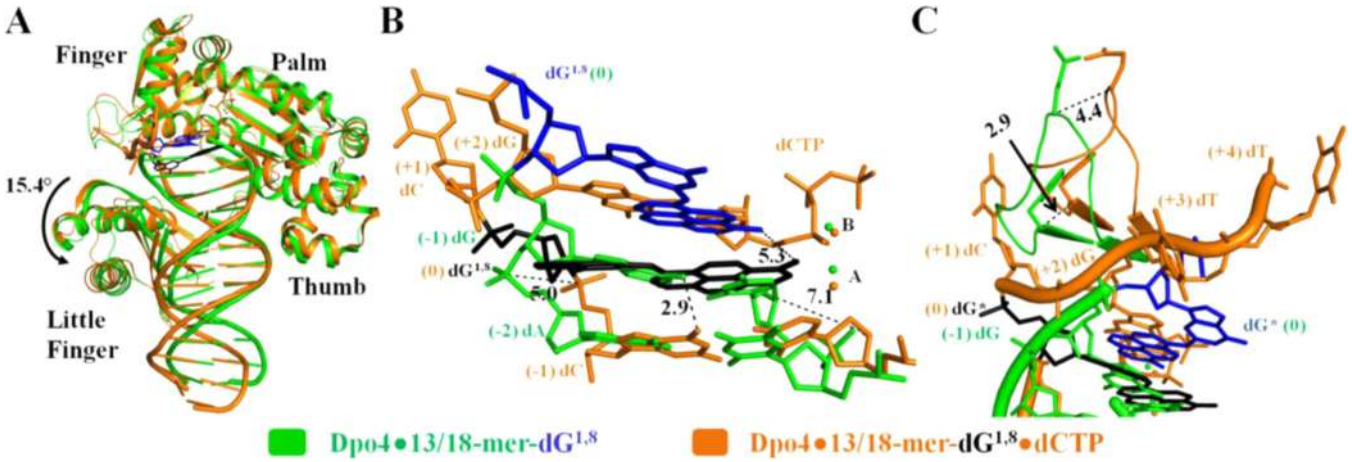

Figure 6.

Overlaying of the Dpo4·13/18-mer-dG^{1,8} and Dpo4·13/18-mer-dG^{1,8}·dCTP crystal structures. (A) Overall superposition of the Dpo4·13/ 18-mer-dG^{1,8} structure (green/blue) with the Dpo4·DNA-dG^{1,8}·dCTP structure (orange/black). Domain names for Dpo4 are labeled. (B) Zoomed view of superimposed active sites. dG^{1,8} lesion has to be translocated by one base pair in order to create space for the binding of dCTP, which forms a Watson–Crick base pair with dG at template position +2. The lesion is sandwiched between the nascent and the primer/template junction base pair. (C) Zoomed view of the structural differences in the binary and ternary complexes. Structural differences are shown as dashed lines with distances in Angstroms.

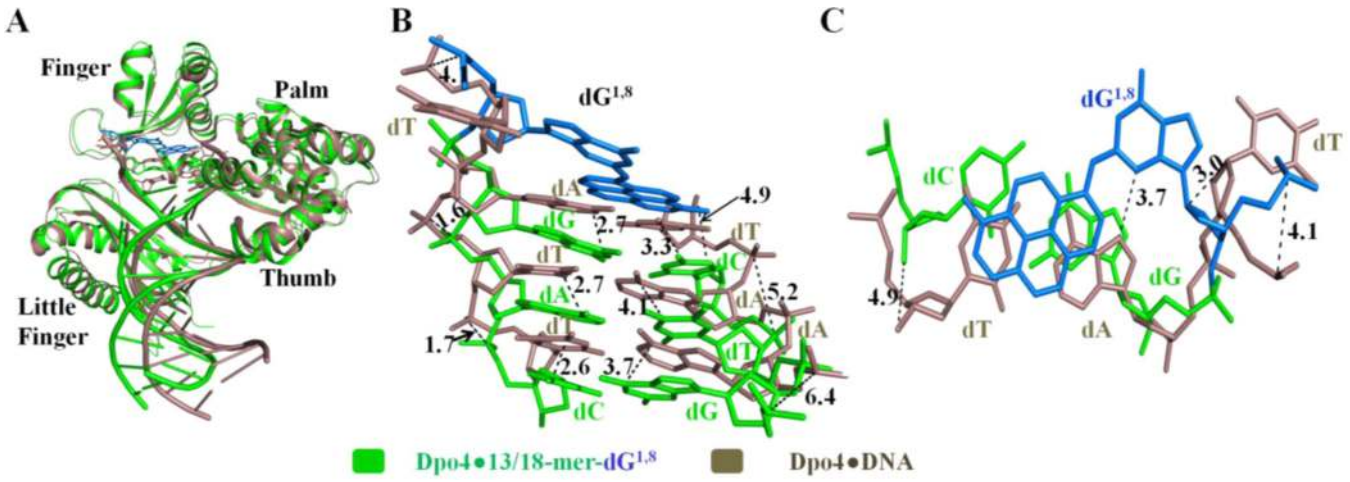

Figure 7.

Comparison of the crystal structures of Dpo4·13/18-mer-dG[1,8] and Dpo4·DNA. (A) Superposition of the Dpo4·13/18-mer-dG[1,8] structure (green/blue) with a previously reported binary structure with undamaged DNA (2RDJ; dirty violet). The name of each Dpo4 domain is labeled. (B) Zoomed view of the superposed active sites in Dpo4·13/18-mer-dG[1,8] and Dpo4·DNA. (C) Zoomed view of the superimposed primer/template junction base pairs and the templating nucleotides dT in undamaged DNA and the dG[1,8] lesion in 18-mer-dG[1,8]. Structural differences in the two structures are shown as dashed lines and measured in Angstroms.

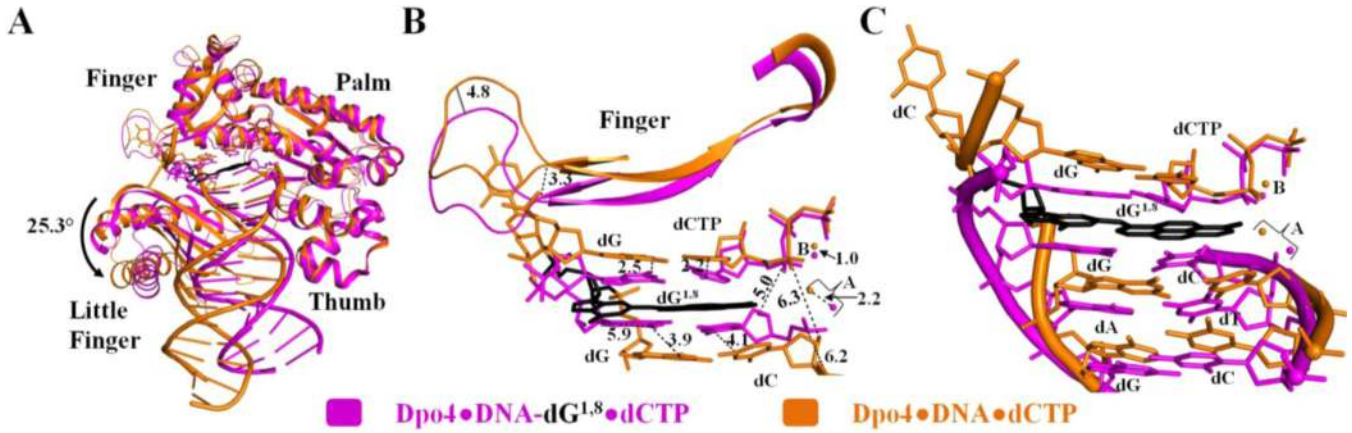

Figure 8.

Overlaying of Dpo4·13/18-mer-dG^{1,8} and Dpo4·DNA·dCTP crystal structures. (A) Overall superposition of the ternary structures of Dpo4·13/18-mer-dG^{1,8}·dCTP (magenta/black) and Dpo4·DNA·dCTP (4QW8; orange). Dpo4 structures are presented as cartoons with labeled domain names. (B) Zoomed view of the superposition of the active sites with a small portion of the Finger domain in cartoon forms. (C) Zoomed view of the superposition of the nucleotides at the active sites. The two Ca^{2+} ions at sites A and B are presented as red spheres.

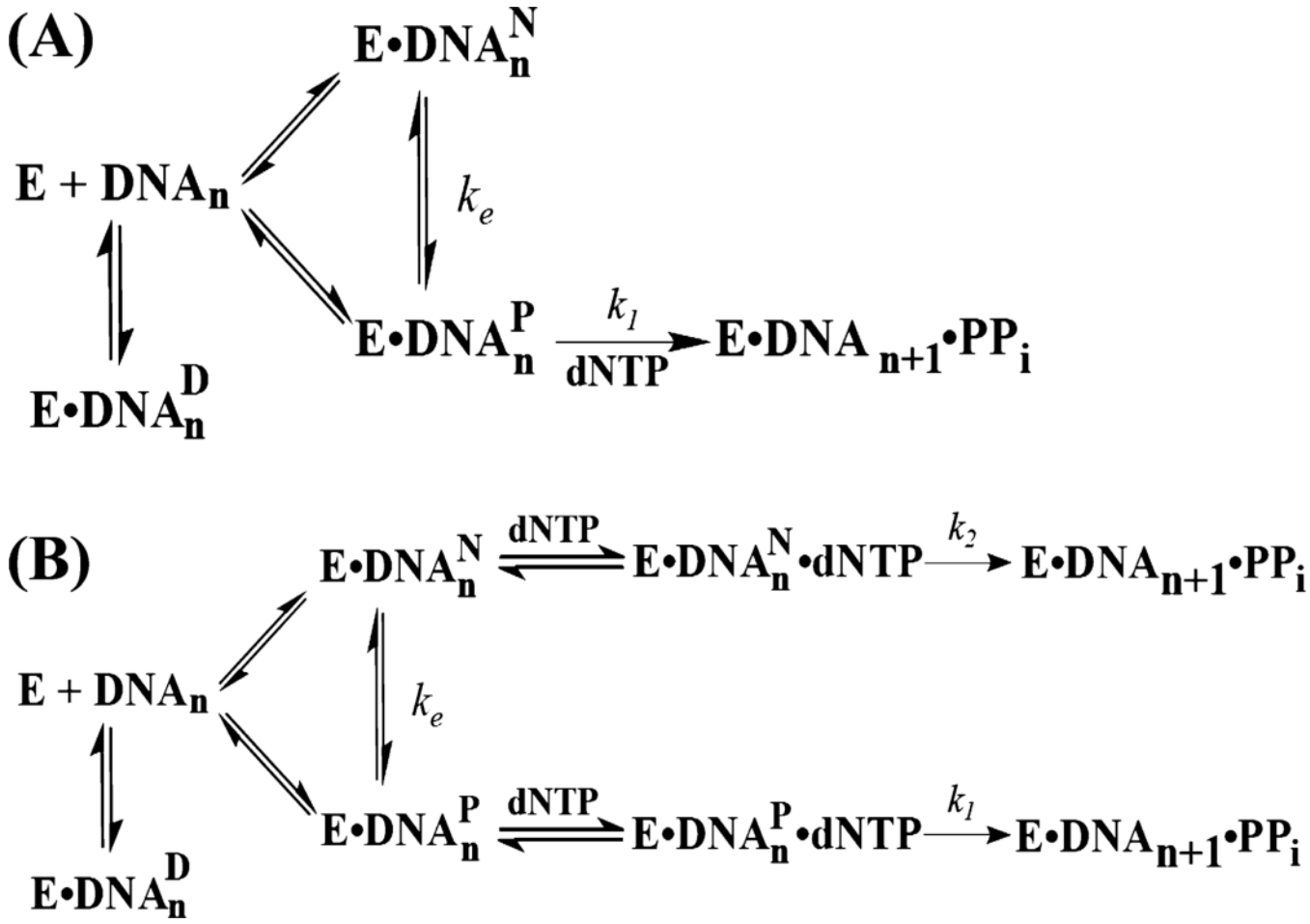

Scheme 1. Proposed Kinetic Mechanisms for Lesion Bypass by Dpo4[a]

[a]E, DNA polymerase; DNA_n, DNA substrate; DNA_{n+1}, extended DNA product by a base; $E{\cdot}DNA_n^N$, nonproductive binary complex; $E{\cdot}\ DNA_n^N{\cdot}$dNTP, nonproductive ternary complex; $E{\cdot}DNA_n^P$, productive binary complex; $E{\cdot}DNA_n^P{\cdot}$dNTP, productive ternary complex; and PP_i, pyrophosphate.

Table 1

Sequences of DNA Oligonucleotides

Primers for kinetic studies	
17-mer	5′-AACGACGGCCAGTGAAT-3′
19-mer	5′-AACGACGGCCAGTGAATTC-3′
20-mer	5′-AACGACGGCCAGTGAATTCG-3′
21-mer	5′-AACGACGGCCAGTGAATTCGC-3′
22-mer	5′-AACGACGGCCAGTGAATTCGCG-3′
Templates for kinetic studies	
26-mer	3′-TTGCTGCCGGTCACTTAAGCGCGCCC-5′
[a]26-mer-dG[1,8]	3′-TTGCTGCCGGTCACTTAAGC***G***CGCCC-5′
DNA Trap	5′-CGCAGCCGTCCAACCAACTCA-3′
D-1 (21/41-mer)	3′-GCGTCGGCAGGTGGTTGAGTAGCAGCTAGGTTACGGCAGG-5′
[b]**DNA oligomers for crystallization**	
Primer 13-mer	1 7 13 5′-CCCAATACCAGTC-3′
Template 18-mer-dG[1,8]	3′-GGGTTATGGTCAG***G***CGTT-5′ -2 0 +2

[a] ***G*** designates dG[1,8].

[b] Nucleotide positions are denoted above the crystallization primer or below the crystallization template.

Table 2

Binding Affinity of Undamaged and Damaged DNA Substrates to Dpo4 at Room Temperature

DNA substrate	$K_{d,DNA}$ (nM) for undamaged DNA[a]	$K_{d,DNA}$ (nM) for damaged DNA[b]	affinity ratio[c]
19/26-mer	3.1 ± 0.5	9.8 ± 0.9	3.2
20/26-mer	4.0 ± 0.2	9 ± 2	2.3
21/26-mer	3.7 ± 0.2	27 ± 3	7.3

[a] Values for K_d,DNA are from ref 41.

[b] Damaged DNA refers to those with template 26-mer-dG[1,8] in Table 1.

[c] Calculated as (K_d,DNA)damaged/ (K_d,DNA)undamaged.

J Am Chem Soc. Author manuscript; available in PMC 2016 September 23.

Table 3

Kinetic Parameters of a Single dNTP Incorporation at 37 °C

dNTP	$K_{d,dNTP}$ (μM)	k_p (s^{-1})	$k_p/K_{d,dNTP}$ (μM^{-1} s^{-1})	efficiency ratio[a]	fidelity[b]	probability[c]
19/26-mer-dG[1,8]						
dGTP	288 ± 63	2.3 ± 0.2	8.0×10^{-3}	3.1		99.7
dATP	571 ± 103	$(7.2 \pm 0.6) \times 10^{-3}$	1.3×10^{-5}	1.1	1.6×10^{-3}	0.2
dCTP	511 ± 148	$(1.4 \pm 0.2) \times 10^{-3}$	2.7×10^{-6}	51.9	3.4×10^{-4}	0.03
dTTP	1799 ± 242	$(1.08 \pm 0.09) \times 10^{-2}$	6.0×10^{-6}	1.5	7.5×10^{-4}	0.07
20/26-mer-dG[1,8]						
dCTP	219 ± 17	$(1.05 \pm 0.03) \times 10^{-2}$	4.8×10^{-5}	1188		93.4
dATP	1149 ± 220	$(1.1 \pm 0.1) \times 10^{-3}$	9.6×10^{-7}	19.8	2.0×10^{-2}	1.9
dGTP	424 ± 90	$(1.7 \pm 0.1) \times 10^{-4}$	4.0×10^{-7}	112.5	8.3×10^{-3}	0.8
dTTP	130 ± 56	$(2.6 \pm 0.3) \times 10^{-4}$	2.0×10^{-6}	41.5	4.0×10^{-2}	3.9
21/26-mer-dG[1,8]						
dGTP	681 ± 130	$(1.9 \pm 0.2) \times 10^{-1}$	2.8×10^{-4}	13.2		97.9
dATP	1630 ± 253	$(1.0 \pm 0.1) \times 10^{-3}$	6.1×10^{-7}	3.9	2.2×10^{-3}	0.2
dCTP	2007 ± 207	$(8.6 \pm 0.6) \times 10^{-3}$	4.3×10^{-6}	7.2	1.5×10^{-2}	1.5
dTTP	937 ± 36	$(9.8 \pm 0.2) \times 10^{-4}$	1.0×10^{-6}	1.8	3.6×10^{-3}	0.4
22/26-mer-dG[1,8]						
dCTP	458 ± 87	2.3 ± 0.2	5.0×10^{-3}	6.8		99.5
dATP	1009 ± 317	$(4.2 \pm 0.7) \times 10^{-3}$	4.2×10^{-6}	1.0	8.4×10^{-4}	0.1
dGTP	273 ± 20	$(3.3 \pm 0.1) \times 10^{-3}$	1.2×10^{-5}	0.71	2.4×10^{-3}	0.2
dTTP	1352 ± 181	$(1.3 \pm 0.1) \times 10^{-2}$	9.6×10^{-6}	1.1	1.9×10^{-3}	0.2

[a] Calculated as $(k_p/K_{d,dNTP})_{undamaged}/(k_p/K_{d,dNTP})_{damaged}$. Values for $(k_p/K_{d,dNTP})_{undamaged}$ are from ref 41. "Undamaged" indicates undamaged DNA, while "damaged" denotes DNA containing a template of 26-mer-dG[1,8].

[b] Calculated as $(k_p/K_{d,incorrect\ dNTP})_{damaged}/[(k_p/K_{d,correct\ dNTP})_{damaged} + (k_p/K_{d,incorrect\ dNTP})_{damaged}]$.

[c] Calculated as $((k_p/K_{d,dNTP})_{damaged}/[\Sigma(k_p/K_{d,dNTP})_{damaged}]) \times 100$.

Table 4

Biphasic Kinetic Parameters for Correct dNTP Incorporation onto 5′-[^{32}P]-Labeled DNA (30 nM) in the Presence of an Unlabeled DNA Trap (5 μM) at 37 °C

DNA substrate	correct dNTP	A_f (nM)[a]	k_f (s^{-1})	A_s (nM)[a]	k_s (s^{-1})
19/26-mer	1.2 mM dGTP	26.7 ± 0.7 (89%)	1.8 ± 0.2		
20/26-mer	1.2 mM dCTP	26.0 ± 0.6 (87%)	2.8 ± 0.3		
21/26-mer	1.2 mM dGTP	25.2 ± 0.6 (84%)	0.49 ± 0.04		
19/26-mer-dG[1,8]	1.2 mM dGTP	22.9 ± 0.6 (76%)	0.74 ± 0.06		
20/26-mer-dG[1,8]	0.2 mM dCTP	5.4 ± 0.5 (18%)	0.014 ± 0.003	18.7 ± 0.9 (62%)	$(2.4 \pm 0.4) \times 10^{-4}$
	0.7 mM dCTP	5.6 ± 0.4 (19%)	0.039 ± 0.007	18.1 ± 0.6 (60%)	$(4.6 \pm 0.4) \times 10^{-4}$
	1.2 mM dCTP	5.4 ± 0.5 (18%)	0.043 ± 0.007	18.2 ± 0.5 (61%)	$(1.9 \pm 0.1) \times 10^{-3}$
21/26-mer-dG[1,8]	1.2 mM dGTP	24.4 ± 0.4 (81%)	0.075 ± 0.005		

[a]Calculated as (reaction amplitude/30 nM) × 100.

Table 5

Data Statistics for the Crystal of the Complexes of Dpo4 and 13/18-mer-dG[1,8] in the Presence or Absence of dCTP

space group	***P*3$_1$**
cell dimens	
a, b, c (Å)	56.39, 56.39, 288.77
α, β, γ (deg)	90.00, 90.00, 120.00
refinement	
resolution (Å)[a]	50.00–2.20 (2.28–2.20)
R_{merge}[b]	14.30 (83.90)
I/σ (I)	11.34 (3.11)
completeness (%)	99.8 (100.00)
redundancy	5.80 (6.80)
resolution (Å)	20.23–2.20 (2.25–2.20)
no. of reflns	49 297 (2649)
R_{work}/R_{free}[c]	0.2015/0.2500
no. of atoms	
protein	5516
DNA-dG[1,8]	1225
dCTP	28
B factors	
protein	43.21
DNA-dG[1,8]	48.96
dCTP	30.2
rms deviations	
bond lengths (Å)	0.008
bond angles (def)	1.294

[a] Highest resolution shell is shown in parentheses.

[b] $R_{merge} = \Sigma|I - \langle I\rangle|/\Sigma I$, where I is the integrated intensity of each reflection.

[c] R value = $\Sigma \parallel F_O| - |F_C \parallel /\Sigma|F_O|$, where F_O and F_C are observed and calculated structure factor amplitudes, respectively.